

Numerical Characterisation of Ship-Airwake Effects on Medium-Weight UAV Approach and Go-Around Operations to Canberra-Class LHDs

Matthew J. Ericksen & Nicholas J. Lawson

School of Aerospace, Mechanical and Mechatronics Engineering, The University of Sydney, Camperdown, NSW 2006, Australia

Abstract

This study characterises the airwake environment faced by medium-weight, conventional take-off and landing UAS within approach and go-around corridors of Canberra-class LHDs. The study focuses on flow asymmetry, incident velocity gradients, and related operational stability and controllability issues. Unsteady CFD simulations were performed on a simplified ship geometry using universal flows between 15 and 35 kts. The results show that ramp-generated vortices, detaching recirculating bubbles, and island boundary flow separation create asymmetric disturbances along both approach and go-around paths, affecting aircraft lift. Lift disparity across these paths suggests that a notional aircraft may experience a roll tendency and loss of lift toward the ship late in the approach, and an opposite roll tendency and lift increase during go-around. These findings indicate that flows from Canberra-class LHDs may demand alternating stability and control requirements on CTOL UAS during critical approach operations near the ship, supporting the need for future flight-dynamic and design-response modelling.

Keywords: Computational fluid dynamics; ship airwake; LHD; UAV-ship recovery; IDDES

1. Introduction

The airwake in the lee of an aircraft carrier is highly disturbed, energetic, and spatially complex flow structures resulting from freestream airflow interacting with bluff bodies, sharp edges, and discontinuities in the ship's geometry. Such turbulent flow fields are known to adversely affect the performance and handling qualities of aircraft operating downwind of the vessel during landing maneuvers [1], when vehicles are flown at low airspeeds and close to their aerodynamic limits. This flight profile is particularly critical, as turbulence affects aerofoil performance at high angles of attack, where stall margins are reduced [2]. These effects are intensified by the ramp structure on ski-jump-equipped vessels, which serves as a dominant bluff body above the flight deck, introducing additional flow separation and recirculation. For ships without angled landing decks, these ramp generated flows can extend across the entire operational envelope of the flight deck [3].

In concert with the increased deployment of ski-jump-equipped vessels, research into carrier operations with uncrewed aerial systems (UAS) has also shifted. Developments range from compact systems designed for helicopter decks to the arrested (cable-assisted) recovery of the X-47B UAS aboard a Nimitz-class supercarrier. These advances show growing momentum for UAS integration in naval aviation. Governments and naval forces worldwide are increasingly interested in the feasibility, operational value, and design requirements—such as launch and recovery methods—of these systems for use on aircraft carriers. In September 2023, the British Royal Navy successfully demonstrated the conventional recovery of a small fixed-wing UAS aboard HMS Prince of Wales [4], as a proof of concept for the operation of lightweight Conventional Take-off and Landing (CTOL) UAS from Short Take-off Vertical Landing (STOVL) carriers.

However, gaps remain in understanding the effects of atmospheric and ship-induced flow fields on UAS performance. Since an uncommanded roll event of an MV-22 Osprey aboard USS Saipan (LHA-02) [5], numerical studies of aircraft and landing helicopter dock (LHD) ship airwakes have grown.

Nevertheless, most published studies have focused on flows above the flight deck and in the immediate hover regions, while conventional straight-in approach and go-around corridors are still largely unstudied. As a result, knowledge of the feasibility and safety margins for lighter, fixed-wing aerial vehicles in these environments continues to be limited. Currently, publicly available studies for fixed-wing UAS approach and go-around corridors aft of LHD geometries are few, especially where the aircraft operates through the combined ramp, island, and stern wake.

Addressing this knowledge gap, this paper presents an initial unsteady Computational Fluid Dynamics (CFD) analysis of a Canberra-class LHD airwake. It identifies flow features relevant to CTOL UAS approach and go-around operations. The unsteady model results characterise ship airwakes and provide valuable insight into the dynamic interactions between the flow field and the UAS. These wake data are intended to support future flight-dynamic response estimation and Multi-disciplinary Design Optimisation Analysis (MDOA) for fixed-wing UAV operations to the ship.

2. Numerical Method

Ansys Fluent 2024R1 was used for all CFD simulations. Because all examined flow speeds were below Mach 0.3, the flow was treated as incompressible and solved using the unsteady pressure-based solver.

The governing flow field was represented using the incompressible Reynolds Averaged Navier–Stokes equations [Eqs. (1) and (2)]. For unsteady turbulent flow, the instantaneous velocity field was decomposed into a mean component, $\overline{\boldsymbol{U}}$, and a fluctuating component, $\boldsymbol{U}'(t)$, such that $\boldsymbol{U}(t) = \overline{\boldsymbol{U}} + \boldsymbol{U}'(t)$.

$$\nabla \cdot \overline{U} = 0 \tag{1}$$

$$\frac{\partial \overline{\boldsymbol{U}}}{\partial t} + \overline{\boldsymbol{U}} \cdot \nabla \overline{\boldsymbol{U}} = -\frac{1}{\rho}\nabla p + \nabla \cdot (v \nabla \overline{\boldsymbol{U}}) - \nabla \cdot (\overline{\boldsymbol{U}'\boldsymbol{U}'}) + \bar{F}_{b_x} \tag{2}$$

The Reynolds stress term, $\overline{\boldsymbol{U}'\boldsymbol{U}'}$, introduces additional unknowns and therefore requires turbulence closure. The two-equation *k*-ω SST model with Improved Delayed Detached Eddy Simulation (IDDES) shielding was used for this purpose. IDDES uses the local grid spacing to regulate the transition between Reynolds-Averaged Navier–Stokes (RANS) modelling and Large Eddy Simulation (LES) resolution, improving near-wall treatment while reducing premature grid-induced separation [6]. Prior ship-airwake studies by Watson et al. [7], Linton et al. [8], and Cvengros et al. [9] similarly demonstrate that IDDES is suitable for resolving the dominant operationally relevant structures produced by large-scale separation, without requiring full resolution of the viscous sublayer. Further, IDDES was selected to model near-wall regions economically while resolving the dominant separated wake structures in LES-like mode, where the grid permits.

3. Simulation Meshing, Setup and Validation

Airwake generation began with a simplified computer-aided design (CAD) model of the LHD, measuring 230.8 m × 32.0 m × 20.5 m (waterline to flight deck). The geometry was built from shipboard measurements and photographic references. Features smaller than 0.25 m, such as handrails, antennae, and hatch protrusions, were omitted. The same applied to components subject to configuration changes, such as radomes, armaments, and exhaust nozzles, as well as to those regularly moved, such as radars and vehicles. The forward deck crane was also omitted. A flight-deck height of 20.5 m above the waterline was chosen to represent the nominal operating condition, recognising that this height varies with ballast state and water salinity during amphibious operations. The ship model was placed along the Z-axis of the computational domain, whose dimensions were 7.0 L × 2.8 L × 1.0 L (where 1 L is equivalent to one ship-length), with its bow located 2 L downstream of the inlet at X = 0. This domain size allowed full airwake development without boundary interference. The outlet was set at least 1 L downstream from the start of the approach corridor, approximately 0.25 nmi aft of the ship. Finally, the ocean surface was treated as a moving wall, with velocity and direction matching those of the ship.

Because the study focuses on corridor-scale separated airwake structures rather than skin-friction prediction, near-wall resolution on the ship was not treated as the primary validation metric. A sensitivity study by Shipman et al. [10] demonstrated that resolving the viscous boundary layer on full-scale ship geometries has a negligible impact on the dominant airwake characteristics, which are instead governed primarily by the inertial effects of flow interaction with bluff-body features. Consequently, to optimise computational efficiency, the mesh was grown from the ship surface with a maximum expansion ratio of 1.2, and inflation layers were applied only at the ocean surface to support development of the atmospheric boundary layer. This approach is appropriate for resolving dominant wake topology, but not for predicting ship-surface skin friction or detailed viscous sublayer behaviour.

The minimum grid spacing was set to 0.25 m at the ramp leading edge, increasing to 0.75 m over the flight deck and further expanding to 1.0 m along the approach corridor. The resultant mesh comprised approximately 6.63 million polyhedral cells, with refinement concentrated around the ship and approach path as shown in Figure 1. Although inflation layers were not used to explicitly resolve the ship's viscous boundary layer, a Courant-Friedrichs-Lewy nubmer ≤ 5 was targeted, with values < 10 considered acceptable, given the use of enhanced wall treatment in ANSYS Fluent and the study's emphasis on inertially driven wake structures.

The numerical setup was validated at wind-tunnel scale, following experiments by Bardera-Mora et al. [11]. Flow parameters were adjusted to match the experimental Reynolds number, and steady-state solutions were computed, consistent with the reported time-averaged measurements. The simulations showed good agreement with the experimental primary flow features, especially the separation and reattachment locations of the recirculation region aft of the ramp.

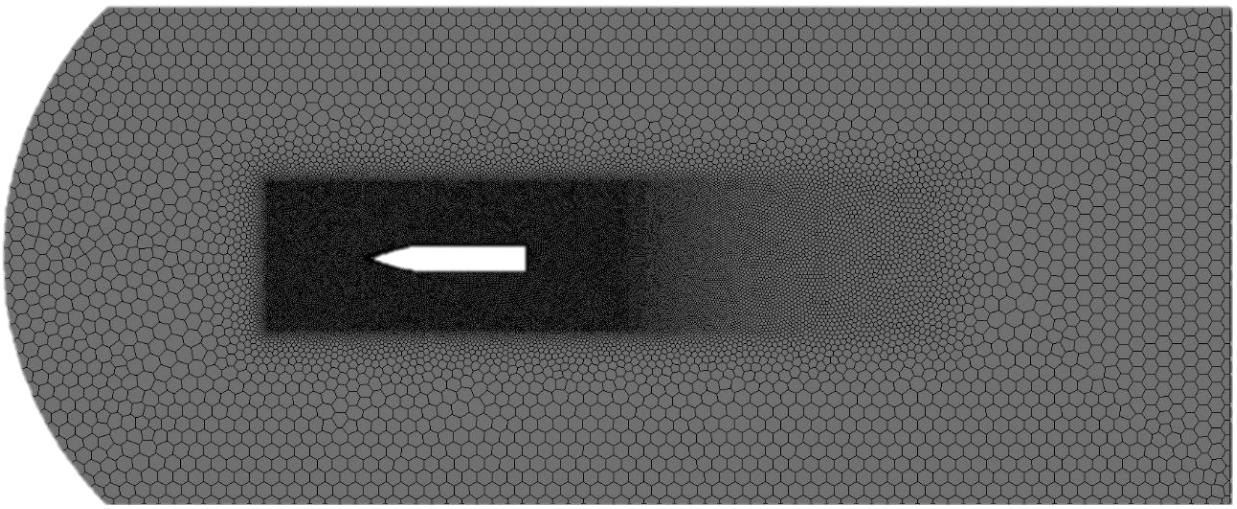


Figure 1 – Simulation domain floor Z = 0 (ocean) surface mesh for 6.63×10^6 cell domain

Spatial grid independence was evaluated under wind tunnel conditions using very fine, fine, medium and course mesh resolutions of 14.0×10^6, 9.07×10^6, 6.63×10^6, and 1.20×10^6 cells. For each mesh, normalised velocities 2 m above the flight deck and ramp were compared with those reported by Bardera-Mora et al. at equivalent locations. The medium refinement best balanced agreement with experimental velocity trends, solution stability, and computational cost. Temporal independence was assessed with time steps of 0.0075, 0.01, 0.02, and 0.03 s using the accepted mesh. Normalised mean velocities along the flight deck centreline were then compared to the measurements of Bardera-Mora et al., showing good agreement in magnitude and trends. Minimal variance among the three smallest time steps indicated temporal convergence, so a Δt of 0.01 s was chosen for full-scale simulations.

Following verification, full-scale airwake simulations were performed with an ambient ocean wind speed of 15 kts. Ship speeds ranged from 0 to 20 kts, with combined Winds over Deck (WOD) between 15 and 35 kts. A flow development period of 2.5 freestream transits was simulated. Velocity data was extracted along the approach and go-around corridors at uniform intervals during a 20 s transient window. This 20 s duration corresponds to the time required for an aircraft flying at 80 kts to traverse

a 0.25 nmi approach in steady 35 kts conditions.

As a secondary full-scale consistency check, the Strouhal number of vertically oriented vortices shedding from the full-scale ship sides was computed. The focus was on the 35 kts case to ease the development and identification of the appropriate vortices. As shown in Figure 2, for a flow progressing from bottom to top, the starboard wake is dominated by negative Z-vorticity structures, while the port-side wake is dominated by positive Z-vorticity structures, indicating an alternating wake pattern. As described by Buresti [12], identifying and classifying shed vortical bodies is difficult in the energetic, complex wakes generated by bluff bodies.

With an average same-sign vortex spacing of approximately 3.5 B (where B is the ship's beam width) and a convection speed of approximately 12.8 ms^{-1}, the large-scale shedding frequency was estimated as approximately 0.11 Hz. Using the ship's beam of 32 m as the defining length, the Strouhal number was calculated to approximate St = 0.2 to 0.21, at $Re \approx 34.4 \times 10^6$.

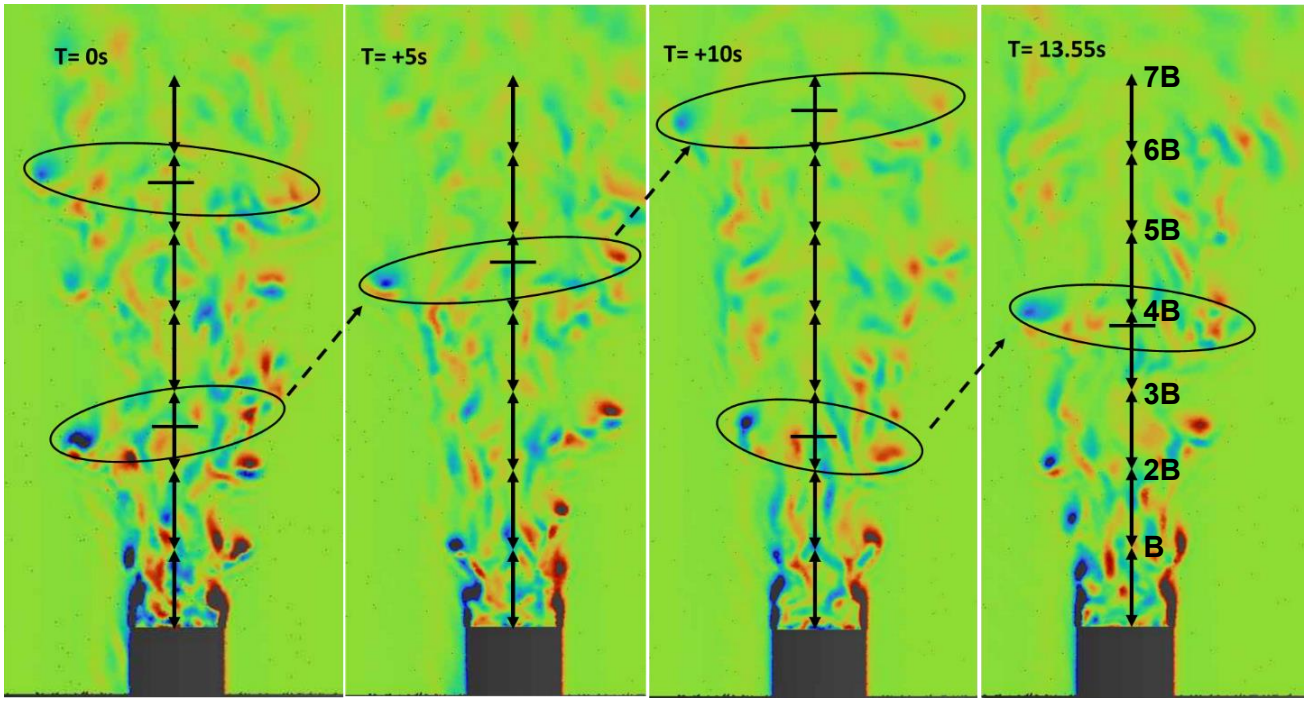


Figure 2 – Temporal comparison of +Z (red) and -Z (blue) vortical body formations behind the ship, 5 m above the ocean surface.

This St is considerably higher than the 0.1 – 0.15 typically expected for a rectangular prism in a laminar flow medium. As Derakhshandeh and Alam [13] highlight, few studies exist for square and rectangular bodies in supercritical flow regimes ($Re > 1.0 \times 10^6$). Roshko [14] is among the few to report a St of about 0.27 for a cylinder at $Re \approx 40 \times 10^6$. Sharp edges and the turbulent boundary layer along the ship's side, leading to separation, which may increase vortex shedding frequency [15]. Thus, $St \approx 0.2$ serves as a reasonable beam-based check for the full-scale wake.

4. Results and discussion

4.1 General

Figure 3 illustrates three dominant flow structures generated by the interaction between the incoming flow and the bow ramp. The port-side vortex is the most intense, driven by the ramp's lateral offset from the ship's centreline. The asymmetric bow geometry directs more incoming flow toward the port side, allowing it to spill over the ramp. The resulting vortex stays attached to the port-side ramp edge until the freestream flow hits the forward face of the island superstructure. At this point, it is pushed outward and begins to spiral downstream.

A centrally located recirculation region forms immediately aft of the ramp and oscillates in both size and strength within the forward third of the ramp length. During each oscillation cycle, packets of

detached turbulent flow, hereafter referred to as burbles, traverse downstream along the deck centreline. These burbles move at approximately the height of the ramp's forward edge (round-out).

The starboard-side vortex is weaker than its port-side counterpart, but is sustained by the adverse pressure gradient behind the ramp and the upwelling flow from the starboard bow working deck. This deck also sheds intermittent turbulent structures that interact with the vortex and strengthen it. Downstream, the island superstructure significantly alters the starboard wake topology. It largely breaks the ramp-generated vortices, replacing them with structure-induced eddies that shed downstream, maintain an almost constant elevation and gradually dissipate into larger, weaker flow features that carry into the wake of the ship.

Detached ramp burbles periodically energise the island-separated flow, producing oscillatory port-side turbulent structures as they convect along the deck. The already turbulent flows are further complicated by the ship's rearward step to the hangar deck, creating the first of the stern recirculation areas and drawing flow from above and around the sides, where the weakened port-side ramp vortex appears to be drawn back toward the approach corridor.

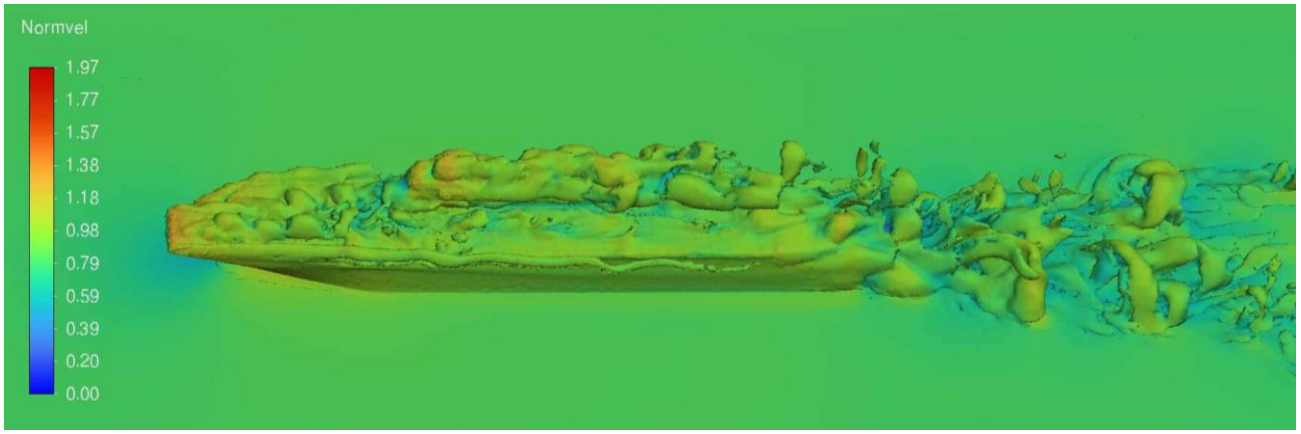


Figure 3 – 1.5 Hz vorticity isosurface, coloured by normalised velocity magnitude, for the 35 kts U_∞

The ship fan wake is a complex arrangement of coherent and incoherent vortex bodies trailing a recirculation and shear wake region behind the ship. The near wake region is a tangle of separated shear-layer structures leading to larger shed wake vortices beyond 2 B downstream.

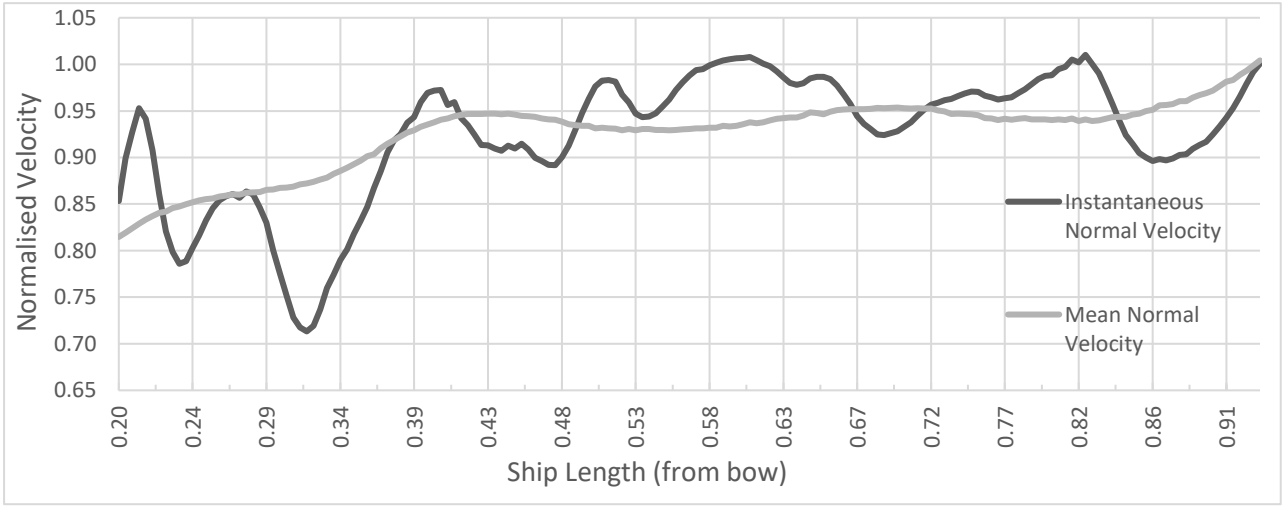


Figure 4 – Velocity variation along deck

Data from sample points located 2 m above the flight deck along the landing centreline, extending from the aft edge of the bow ramp to the stern, showed several consistent trends, as seen in Figure 4.

Overall, the mean velocity magnitude increases with downstream distance from the ramp. After an initial region of highly unsteady flow immediately aft of the ramp, the velocity field generally stabilises along the length of the island superstructure before reaccelerating toward freestream conditions near the stern. Notably, the vorticity magnitude exhibits a sharp reduction from approximately 1.5 to 0.5 s^{-1} at about 0.45 L from the bow, corresponding to the aft edge of the island flight control overhang. At this same location, turbulence intensity decreases by nearly 50% before gradually increasing downstream, reaching approximately 0.3% at the fantail.

4.2 Approach Corridor

The approach corridor begins at a touchdown point approximately 35 m forward of the flight-deck stern edge (to provide sufficient clearance for aircraft to land forward of the aft aircraft elevator) and extends 0.25 nmi aft along a 4° slope above the horizon. The corridor extends 16.25 m on either side of the landing-area centreline, corresponding to a ±2° guided approach at 0.25 nmi. Extending the width beyond this was considered inefficient as effects on the slope weren't likely to be experienced until just above ship height.

As such, it was observed through each simulation that the ship wake effects became significant approximately 2/3 L aft of the stern (as illustrated in Figure 5), where the 4° approach slope is approximately level with the mid-height of the island masts. That said, slowly convecting wake structures were able to reach as high as the mast tops, as expected. Further, the majority of the flow disturbance along the slope is toward the starboard side of the corridor as a direct result of the bluff body separation of the island wake. The intensity of these flows increases with proximity to the ship, while exhibiting alternating vortex shedding behaviour reminiscent of a von Kármán wake, before becoming further destabilised with increasing distance behind the island. As per the bodies identified in the general observations, the ramp's port side vortex then influences the port side of the slope corridor flow at a height just above the ramp peak, while the separation and boundary flows of the deck, including the aft convecting burble, intersect the slope in close proximity to the ship.

As the universal flow speeds (U_∞) progress from 15 kts to 35 kts (7.71 to 18.01 ms^{-1}, respectively), we see not only the expected intensification of turbulent bodies in the final approach stages of the corridor, but also the expansion of their influence on the slope corridor. For instance, at 15 kts, the portside vortex partly affects the slope along the length of the flight deck, while deck boundary layers and residual detached turbulent structures are significant just prior to aircraft touchdown. At 35 kts, these bodies affect the slope an additional beam width rearward, extending several metres behind the ship's stern on the port side.

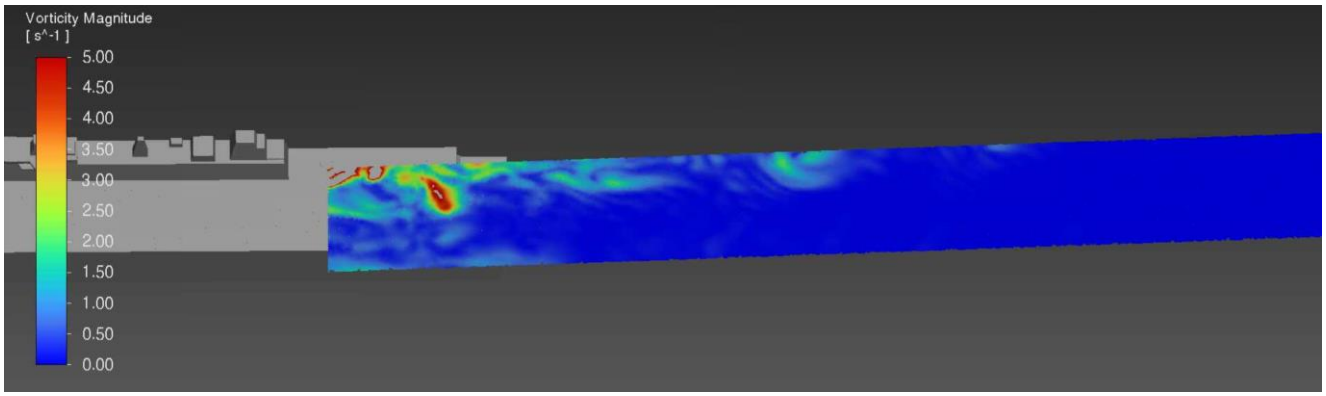


Figure 5 – Instantaneous vorticity magnitude on the 4° approach corridor at 35 kts U_∞

For analysis purposes, three measurement paths were chosen: the centreline of the corridor and 10 m either side. The right corridor wing path was chosen specifically because it provided adequate clearance between the right wing tip and the ship's island should the aircraft approach terminate in a landing.

The normalised mean velocity values across the flow scenarios are very similar, whereas their turbulence intensity and vorticity distributions show distinct differences. In all cases and along each of the analysed wing paths (those being the left, centreline and right), the mean velocities generally increase steadily until a point at, or just behind, the stern of the flight deck, where the ship's profile makes a rearward step 10 m down to the aft work deck/ hangar deck. The change in velocity varies, with the centreline peaking at approximately 1.05 U_∞. Behind the peak, the normalised velocity decreases sharply, partially or fully offsetting the preceding acceleration along the flight deck. The right wing path reaches a minimum around 20 m behind the ship's stern at approximately 0.873 U_∞, while the centre and left wing path trough around 40 m behind at similar values around 0.976 U_∞. From here, all three wing path velocities gradually increase at varying rates, eventually converging near 1 L behind the stern at just above U_∞ and continuing to subtly increase with distance because of the global atmospheric boundary.

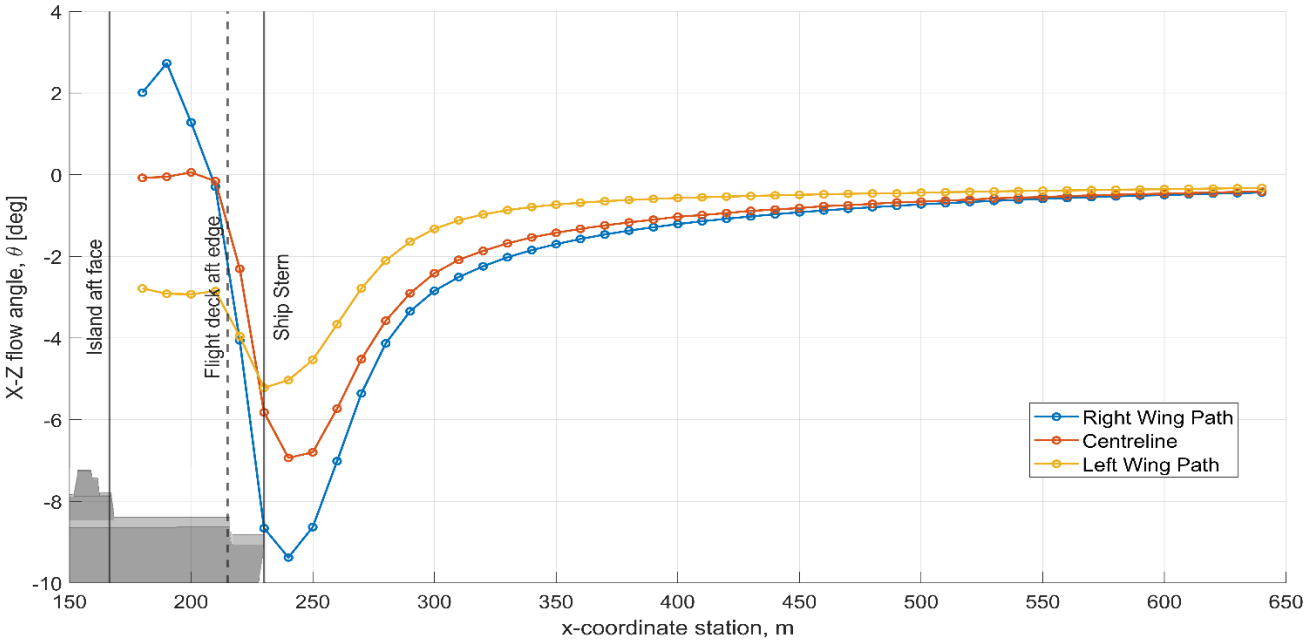


Figure 6 – Local vertical inclination of the X–Z flow vector along the approach corridor at 35 kts U_∞

The incident flow angle shows similar trends across the three measurement paths. We see in Figure 6 the right measurement path, nearest the island wake, exhibits the largest angular variation, while the left path shows the smallest. All three experience their greatest negative value either at or just behind the ship's stern. The left wing path starts at an angle below the horizon, likely as a result of the inward turning effect of the port side ramp vortex, while the others start around their max. The right-wing path shows the largest drop of the three, from approximately 2.73° to -9.37°.

For an aircraft maintaining a nominal 3° pitch attitude on a 4° approach slope, the local flow-angle variation would be expected to reduce the effective angle of attack and produce asymmetric lift across the sampled paths from a position approximately 0.5 L from the touchdown point. The estimated lift differential between the left and right measurement paths shows a likely right-roll tendency during the final approach segment, followed by a reversal in the inferred roll tendency and recovery of lift generation near the shipstern. This downwash within 0.5 L of the ship stern is a known condition to carrier aviation approaches [16]; however, the right rolling tendency is not usually discussed in the typical studies, possibly because they concentrate principally on vessels whose island is not as proportionally large and thus has a limited overall effect in comparison to the downwash. The combination of downward flow and roll moment may require substantial control input and/or lift augmentation to safely overcome in such a confined approach corridor. Further refinement of the probe distances relative to one another would help obtain precise values and assess the extent to which the flows are affected.

4.3 Go-around Corridor

The go-around corridor starts at a point approximately 6 m aft of the ship's stern and extends forward 199.63 m at a 3.5° angle, consistent with representative instrument missed-approach climb gradients. This slope angle was considered suitable for providing a standard positive rate of climb away from the ship without over-extending the aircraft's pitch angle and risking a stall. The rationale for its placement was to represent a decision point level with the top of the island, followed by a 2-second power response and stabilisation interval before transitioning to the go-around climb path. To simplify data collection, it was assumed that during these 2 seconds, the aircraft would continue descending on the approach path, sinking below the island's top deck, until it intersected the go-around corridor. For continuity reasons, the corridor width on either side of the centreline was kept the same as the approach corridor, as were the three measurement paths.

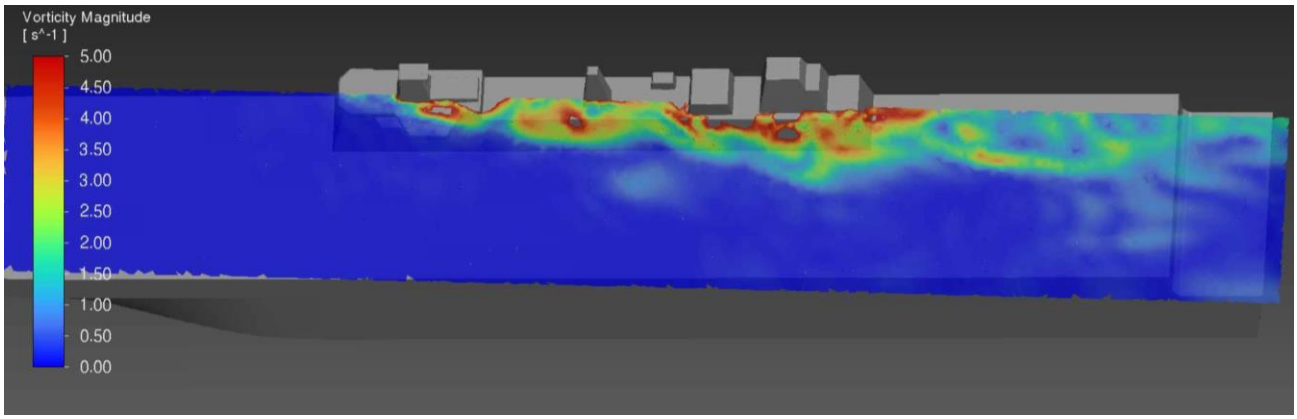


Figure 7 – Instantaneous vorticity magnitude on the 3.5° go-around corridor at 35 kts U_∞

As expected, given its proximity to the go-around corridor, the bluff body separation and shedding of flows from the ship's island heavily impact the starboard side of the corridor, seen below in Figure 7. As its wake trails behind, it expands laterally across approximately half of the corridor width near the go-around entry point. For the most part, the deck boundary layer and ramps' burble don't appear to impact the slope until approximately halfway along the island, to which point, because the rearward extension of the slope lies progressively closer to the deck, the influence of these flow bodies increases. At the aft face of the island, the entirety of the go-around corridor is affected.

At the slower U_∞ of 15 kts, all of the potentially influential bodies reside close to the boundary layer of the bluff bodies. The deck and ramp bodies have only an occasional impact toward the rear of the corridor, principally due to its closer proximity to the deck. The port edge of the go-around corridor appears relatively clear of turbulence or vortical structures for the majority of its length. At the higher U_∞ of 35 kts, the effects are substantial, such that the ramp burble likely influences the central region of the slope parallel to the rear half of the island and further along the flight deck.

A quantitative examination along the three measurement paths shows noticeable similarity in turbulent flow behaviour, with three turbulence-intensity peaks observed along the centreline, concentrated near the island aft face and the flight-deck aft edge, likely driven by flow drawn into the separated regions formed by the rearward steps at these features.

The normalised velocity trends are also similar for all the measured U_∞ scenarios. Generally, the centreline and left-wing paths remain stable for the entire length around 1.025 U_∞, with a slight uptick toward 1.05 U_∞ at the commencement of the go-around corridor. The right-wing path, however, decreases steadily toward 0.725 U_∞ just ahead of the island aft face. From here, it reaccelerates to a peak of 1.09 U_∞ at a point 15 m behind the island bow face, before dropping again to stabilise and converge with the centre and left velocity magnitudes at 1.025 U_∞. As with the approach corridor, values above U_∞ are likely a function of both the ship accelerating the flow around it and the increase of U_∞ with altitude as the corridor climbs through the atmospheric boundary layer.

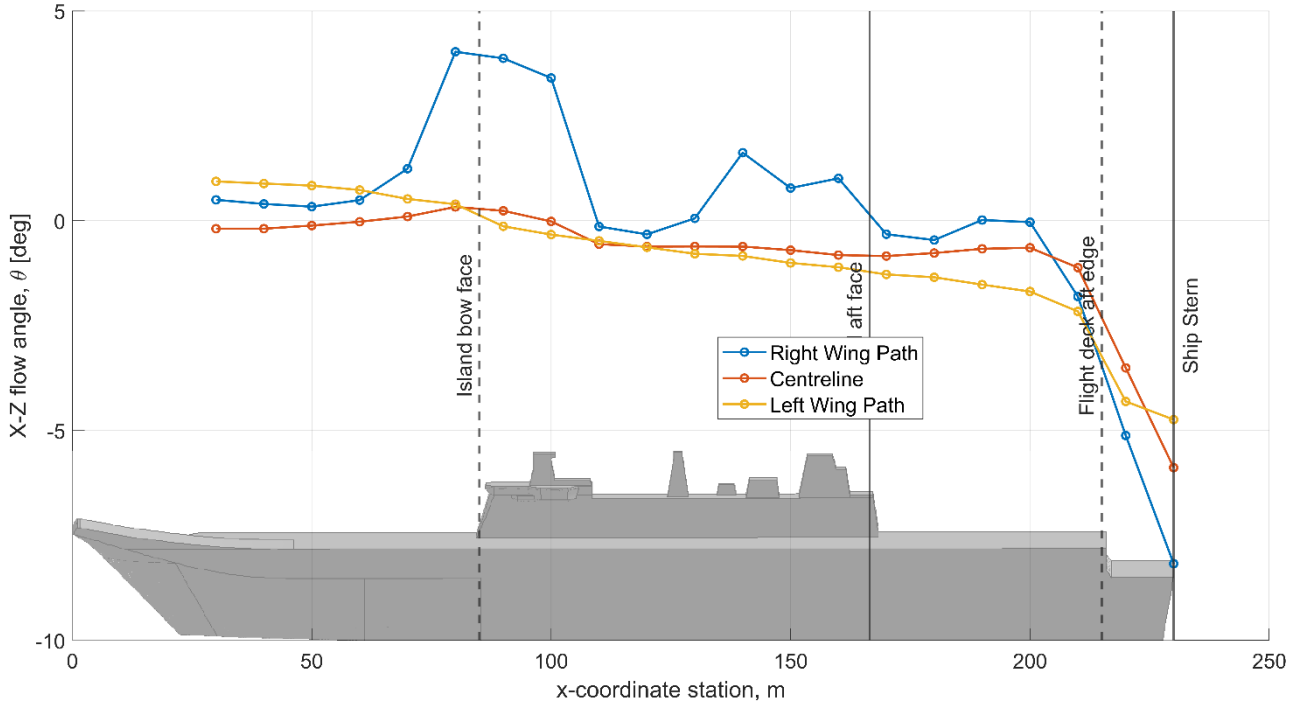


Figure 8 – Flow incident angle along the three go-around measurement paths.

The incident angle of the flow to the horizon shows a similar pattern to the velocity, with the centreline and the left-wing paths generally following each other, varying up to approximately 1°. Each of the flow angles began with a negative angle at the ship's stern, similar to the approach corridor. However, the go-around values increased quickly once over the ship, before stabilising at a point near the forward edge of the aircraft elevator. From here, the centreline and left-wing values increase slowly toward 0. Meanwhile, the right-wing path values oscillated principally in the positive region, reaching a peak of approximately 4.5° just ahead of the island bow face. As evident in Figure 8, the combined effect of the island-induced upwash velocities with wing path incident angles suggests that aircraft would experience a flow induced roll tendency to the left, away from the ship as it climbed the length of the go-around corridor.

4.4 Summary

The simulations show that Canberra-class LHDs generate a highly asymmetric airwake dominated by ramp separation, a strong port-side ramp vortex, and island-induced wake separation in WOD conditions between 15 and 35 kts. These structures extend and expand into the standard approach and go-around paths of CTOL aircraft operating from the ship, with intensity and complexity increasing with U_∞. The approach corridor experiences the greatest disturbance in the final stages of touchdown. Here, reductions in local flow velocity and effective wing angle indicate asymmetric lift, with possible roll tendency toward the island structure. Once over the flight deck stern, velocities generally peak before dropping as the corridor enters the separated deck boundary layer, where wing-in-ground effects could reasonably be considered. The go-around corridor exhibited alternative behaviour. Flows are primarily affected by the island wake, creating an upwelling effect that strengthens near the island and bow. The indicative lift disparity suggests a notional aircraft would tend to roll left, away from the ship, before receiving clean air at just above U_∞. Overall, these alternating lift-effect tendencies could require a reversal in control inputs during a critical flight phase.

Further refinement of the probe spacing would assist in resolving precise values and the degree to which the flows are affected. In addition, modelling of the six-degree-of-freedom ship motion would enable greater definition of flow pumping and shielding, as highlighted by Dooley et al. [17]. This would provide better resolution of wake pumping and shielding effects in the approach and go-around corridors.

5. Conclusions

This study presents full-scale simulations of an LHD operating in combined headwind-ship-speed conditions (U_∞) of 15, 25, and 35 kts. Following validation against experiments by Bardera-Mora et al. [11], and a beam-based Strouhal consistency check for typical bluff bodies at high Reynolds number [14], transient flow data were extracted from the approach and missed-approach corridors over a 20 s sampling window. Each relative wind case was also examined qualitatively to identify the dominant turbulent structures, their spatial evolution, and the underlying mechanisms of their generation.

As anticipated, the bow ramp significantly disrupts the incoming flow over the length of the flight deck. This disruption is driven by an oscillatory turbulent wake (“burble”) convecting downstream and by an intense port-side vortex. The island superstructure further modifies the flow field, largely suppressing the starboard-side vortex and increasing flow complexity along the starboard portion of the landing area, which extends into the approach/missed-approach corridors. Compared to the island wake, the ramp’s direct influence is less pronounced during landing and go-around manoeuvres.

Analysis showed that in the later stages of an aircraft’s approach, the flow velocity and incident-angle distributions indicate a likely reduction in effective lift within 0.5 L of the stern and lift disparity to the right, likely to induce a rapid roll in that direction. Both phenomena are a result of the backward steps at the stern of the ship, and the additionally disruptive effect of the island on the ship's wake. The go-around corridor shows a different response, with relatively steady downward flow across most of the corridor but measurable upwelling on the right side near the island. The resulting lift disparity indicates a potential left-roll tendency away from the ship structure.

Further analysis, with respect to stability and control, will be the subject of a future paper, leading to a greater understanding of UAS performance within the approach, missed-approach, and landing corridors.

6. Contact Author Email Address

For any questions, comments or further discussion, please contact the author via email at:

Mr Matthew J. Ericksen: meri5745@uni.sydney.edu.au

Prof Nicholas Lawson: nicholas.lawson@sydney.edu.au

7. Copyright Statement

The authors confirm that they, and/or their company or organization, hold copyright on all of the original material included in this paper. The authors also confirm that they have obtained permission, from the copyright holder of any third party material included in this paper, to publish it as part of their paper. The authors confirm that they give permission, or have obtained permission from the copyright holder of this paper, for the publication and distribution of this paper as part of the ICAS proceedings or as individual off-prints from the proceedings.

8. References

[1] Polsky S A and Naylor S M. CVN Airwake Modeling and Integration: Initial Steps in the Creation and Implementation of a Virtual Burble for F-18 Carrier Landing Simulations. *Proc AIAA Modelling and Simulation Technologies Conference and Exhibit*, San Francisco, CA, AIAA Paper 2005-6298, 2005.

[2] Anderson J D. *Introduction to Flight*. 8th edition, McGraw-Hill Education, 2016.

[3] Kelly M F, White M D, Owen I and Hodge S J. The Queen Elizabeth Class Aircraft Carriers: Airwake Modelling and Validation for ASTOVL Flight Simulation. *Proc Royal Aeronautical Society Applied Aerodynamics Conference*, 2016.

[4] Royal Navy. Aircraft drone makes history landing on Royal Navy carrier at sea. Royal Navy, 2023. Available from: https://www.royalnavy.mod.uk/news/2023/september/08/20230907-first-aircraft-drone-on-board-hms-prince-of-wales.

[5] Rajagopalan G, Helitek S, Wadcock A J, Yamauchi G K and Silva M J. Experimental and Computational Study of the Interaction Between a Tandem-Rotor Helicopter and a Ship. *Proc 61st Annual Forum of the American Helicopter Society*, Grapevine, Texas, 2005.

[6] Nikitin N V, Nicoud F, Wasistho B, Squires K D and Spalart P R. An approach to wall modeling in large-eddy simulations. *Physics of Fluids*, Vol. 12, No. 7, pp 1629–1632, 2000.

[7] Watson N A, Kelly M F, Owen I, Hodge S J and White M D. Computational and experimental modelling study of the unsteady airflow over the aircraft carrier HMS Queen Elizabeth. *Ocean Engineering*, Vol. 172, pp 562–574, 2019.
[8] Park H S, Linton D and Thornber B. Rotorcraft fuselage and ship airwakes simulations using an immersed boundary method. *International Journal of Heat and Fluid Flow*, Vol. 93, Article 108916, 2022.
[9] Cvengros M. *CFD Simulations of Unsteady LHA Ship Airwake in OpenFOAM*. Master of Science Thesis, KTH Royal Institute of Technology, Stockholm, 2018.
[10] Shipman J, Arunajatesan S, Menchini C and Sinha N. Ship Airwake Sensitivities to Modeling Parameters. *Proc 43rd AIAA Aerospace Sciences Meeting and Exhibit*, Reno, NV, AIAA Paper 2005-1105, 2005.
[11] Bardera-Mora R, García-Magariño A, Rodríguez-Sevillano A and Barcala-Montejano M Á. Aerodynamic Flow Effects on Aircraft Carrier Takeoff Performance. *Journal of Aircraft*, Vol. 56, No. 3, pp 1005–1013, 2019.
[12] Buresti G. Vortex shedding from bluff bodies. *Wind Effects on Buildings and Structures*. Balkema, Rotterdam, pp 61–95, 1998.
[13] Derakhshandeh J and Alam, M. A review of bluff body wakes. *Ocean Engineering*, Vol. 182, pp 475-488, 2019.
[14] Roshko A. Experiments on the flow past a circular cylinder at very high Reynolds number. *Journal of Fluid Mechanics*, 1961.
[15] Knisely C W. Strouhal numbers of rectangular cylinders at incidence: A review and new data. *Journal of Fluids and Structures*, Vol. 4, No. 4, pp 371-393, 1990.
[16] Nelson J. H and Griffin G. M. *United States Navy pilot-controlled landing procedure and associated equipment*. North Atlantic Treaty Organization, Advisory Group for Aerospace Research and Development, 1963.
[17] Dooley G, Ezequiel Martin J, Buchholz J. H. J, and Carrica P. M. Ship Airwakes in Waves and Motions and Effects on Helicopter Operation. *Computers & Fluids*, Vol. 208, 2020.